Electronic Supplementary Material (ESI) for Nanoscale.

A dual-template synergistic assembly strategy towards the synthesis of extra-small nitrogen-doped mesoporous carbon nanospheres with large pores

Caicheng Song[+ a, b], Yiwen Guo[+ c], Tianwei Wang[a], Kun Liu [b, c], Pin-Yi Zhao[b, d, e], Ying Liu[b], He Huang[a], Rongwen Lu*[a] and Shufen Zhang[a]

[a] State Key Laboratory of Fine Chemicals, Frontiers Science Center for Smart Materials, School of Chemical Engineering, Dalian University of Technology, Dalian, 116024, China

[b] SINOPEC, Dalian Res Inst Petr & Petrochem Co Ltd, 96 Nankai St, Dalian 116045, Peoples R China

[c] Institute of Materials and Technology, Dalian Maritime University, Dalian 116026, China

[d] Institute for Materials Discovery, University College London, WC1E 7JE, United Kingdom

[e] Department of Chemistry, University College London, WC1H 0AJ, United Kingdom

[+] These authors contributed equally to this work.

* Corresponding authors.

E-mail address: lurw@dlut.edu.cn

1. Supplementary experiments

Based on the synthesis of NMePS, the key factors involved in the synthesis route were regulated to understand the synthesis method. The specific regulatory content is as follows: keep other conditions unchanged and do not add SO and P123 to the system; Add SO or P123 separately within the system; Change the usage of P123 (SO/P123 with different mass ratios) to 0.01 g (2:1), 0.02 g (1:1), 0.04 g (1:2), 0.06 g (1:3), 0.08 g (1:4), and 0.10 g (1:5), respectively; Change the amount of 3,5-diaminobenzoic acid to 1.0 mmol, 1.4 mmol, 1.8 mmol, 2.2 mmol, 2.6 mmol, and 3.0 mmol, respectively; Replace 3,5-diaminobenzoic acid with equimolar amounts of 2,4-diaminobenzenesulfonic acid for the reaction, and investigate the effect of the reaction system on the sample structure.

Based on the synthesis of NMePS, expand the types of anionic and amphiphilic surfactants to explore the scalability of this synthesis route. Keep the molar amounts of anionic and amphiphilic surfactants at 0.066 mmol and 0.010 mmol, respectively, and change the composition of the composite surfactant to SO-F127, sodium laurate (SL)-P123, sodium stearate (SS)-P123, sodium laurylsulfonate (SLS)-P123, and sodium dodecylbenzenesulfonate (SDBS)-F127.

2. Characterization

SEM images were carried out by the cold field emission scanning microscopes (SU88220) from JEOL. JEOL Model JEM-F200 Fe-SEM system (200 kV) was used to reveal the interior structure of prepared samples, namely, obtain TEM images. The physical adsorption tests were implemented through Beishide Instrument 3H-2000PM.

The X-ray diffraction (XRD) pattern of as-prepared samples was measured by A Rigaku Model D/Max 2400 diffractometer (Cu Kα radiation, λ = 1.5418 Å). The Via Qontor Micro confocal Raman spectrometer was applied to get the Raman spectrum. The Thermo VG ESCALAB 250 equipment was employed to determine the X-ray photoelectron spectroscopy (XPS) analysis. An Elementar Analysensysteme Vairo Macro EL Cube microanalyzer tested the N content of all samples. The functional group information and C atom information (Solid-state ^{13}C cross-polarization magic angle spinning (CP-MAS) NMR spectra) of the polymer precursor are characterized by Thermo Fisher Nicolet iN10 Fourier Transform Microscopic infrared spectrometer (FTIR spectra) and Agilent DD2-500 MHz system (125.7 MHz, with a spinning rate of 10 kHz, 1000 scans, a 4 s pulse delay, and a contact time of 4 ms), respectively. Chemical shift refers to TMS.

3. Electrochemical measurement

The slurry was synthesized from NMeCS (80 wt. %), super P (10 wt. %), and polyvinylidene fluoride (10 wt. %), which was coated on Cu foil and dried at 80 ^{o}C overnight. CR2032 coin-type cells were assembled in an Ar-filled glove box and tested by a Land CT2100 Battery Testing System for electrochemical performance. Li foil was employed as the counter electrode, and 1 M $LiPF_6$ in ethylene carbonate (EC) and diethylene carbonate (DEC) (50:50 v/v) were used as the electrolyte. The schematic representation of coin cell was shown in Scheme S1.

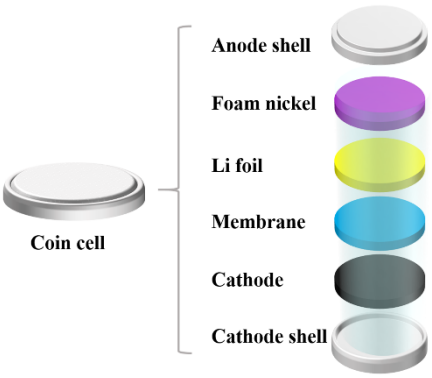

Scheme S1 A schematic representation of coin cell.

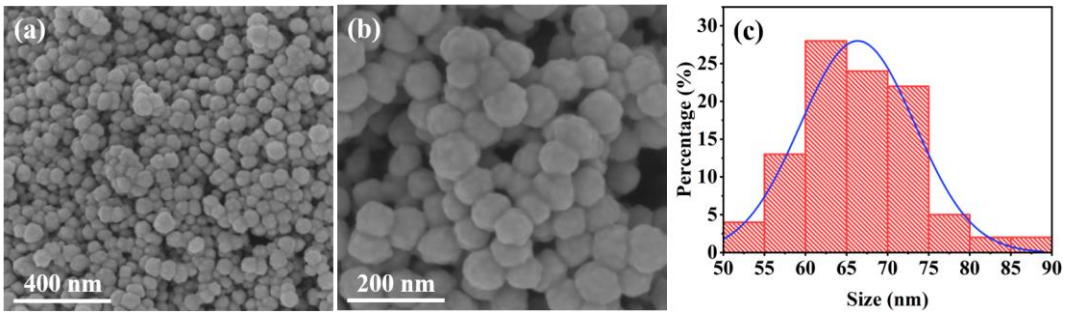

Fig. S1 (a, b) SEM images and (c) particle size distribution of NMePS.

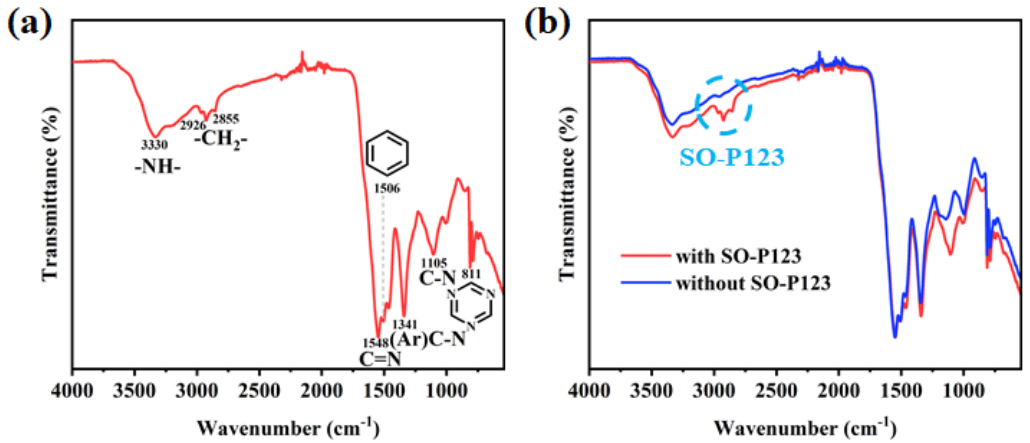

Fig. S2 (a) FTIR spectrum of NMePS and (b) comparison of FTIR spectra between NMePS and NPS.

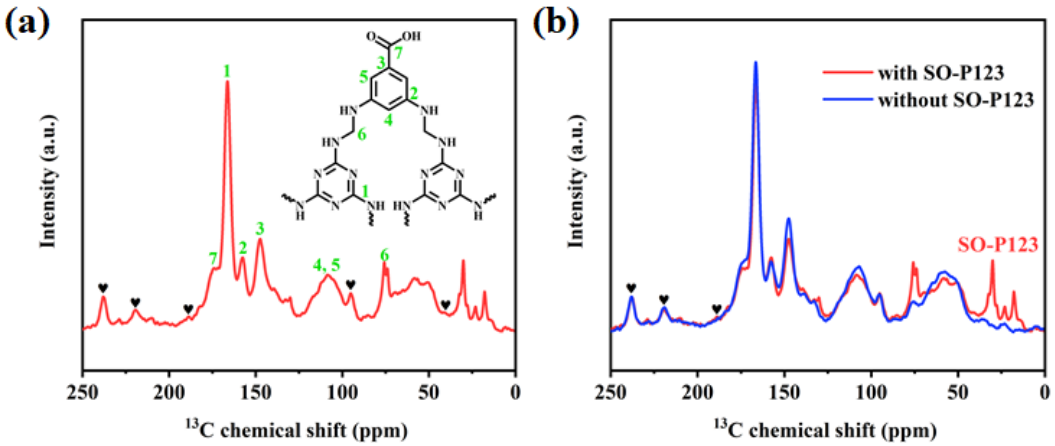

Fig. S3 (a) ^{13}C (CP-MAS) NMR spectrum of NMePS and (b) comparison of ^{13}C (CP-MAS) NMR spectra between NMePS and NPS (the black peaches denote the spinning side bands).

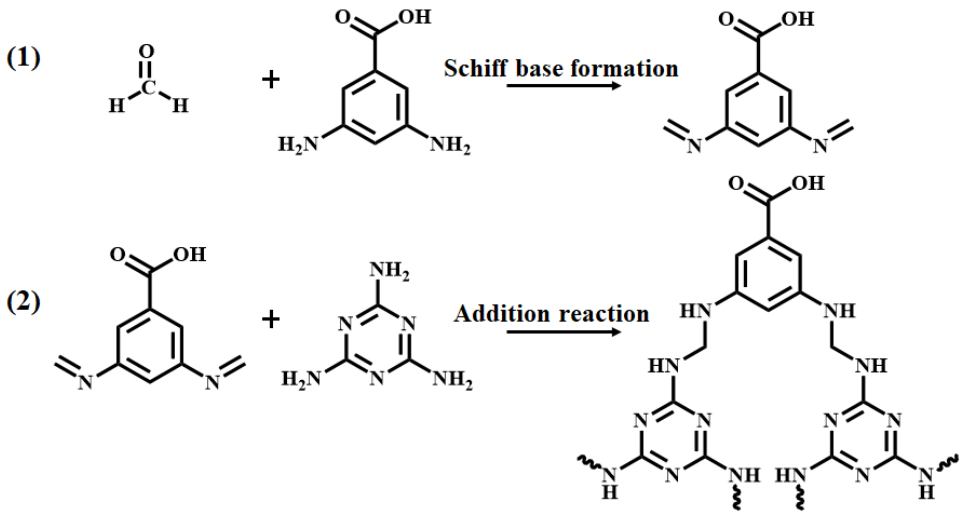

Fig. S4 Possible polymerization reaction mechanism and framework structure of NMePS.

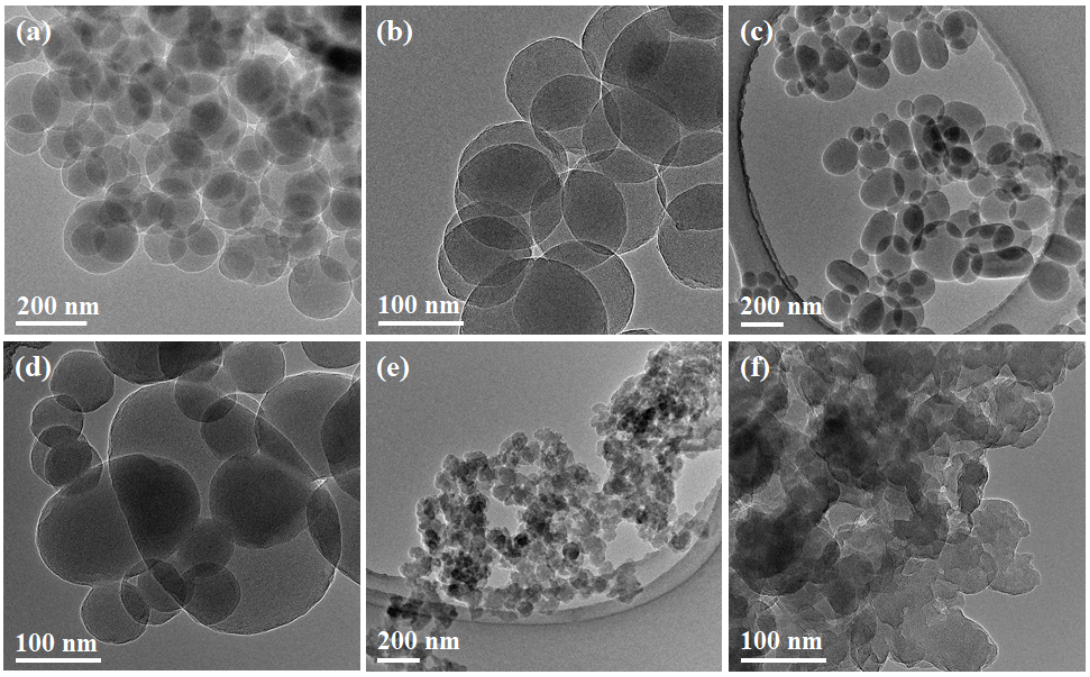

Fig. S5 TEM images of samples prepared by different templates: (a, b) without surfactant, (c, d) using SO alone, and (e, f) using P123 alone.

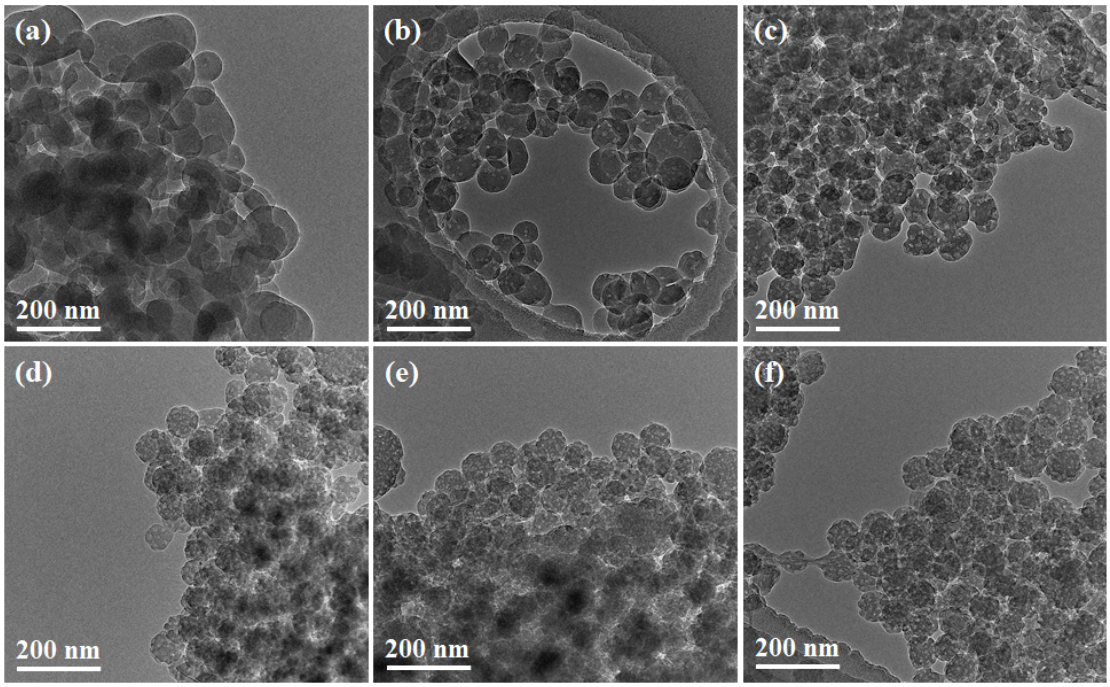

Fig. S6 TEM images of polymeric nanoparticles prepared by SO and P123 with different mass ratios: (a) 2:1, (b) 1:1, (c) 1:2, (d) 1:3, (e) 1:4, and (f) 1:5.

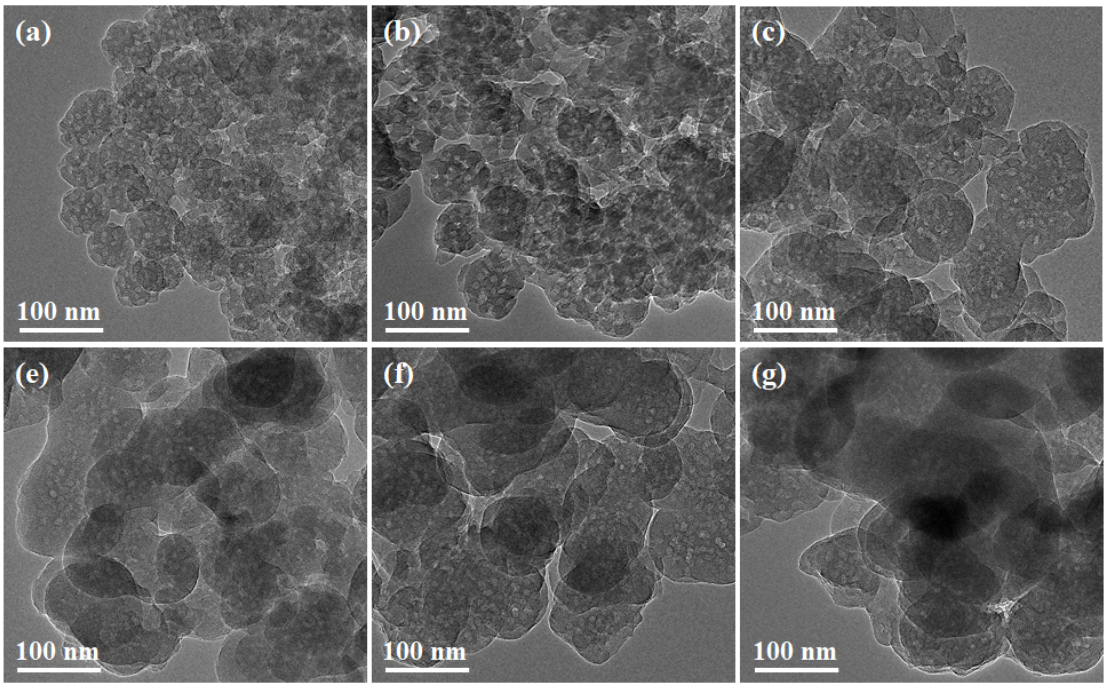

Fig. S7 TEM images of samples prepared with different amounts of 3, 5-diaminobenzoic acid: (a) 0.6 mmol, (b) 1.0 mmol, (c) 1.4 mmol, (d) 1.8 mmol, (e) 2.2 mmol, and (f) 2.6 mmol.

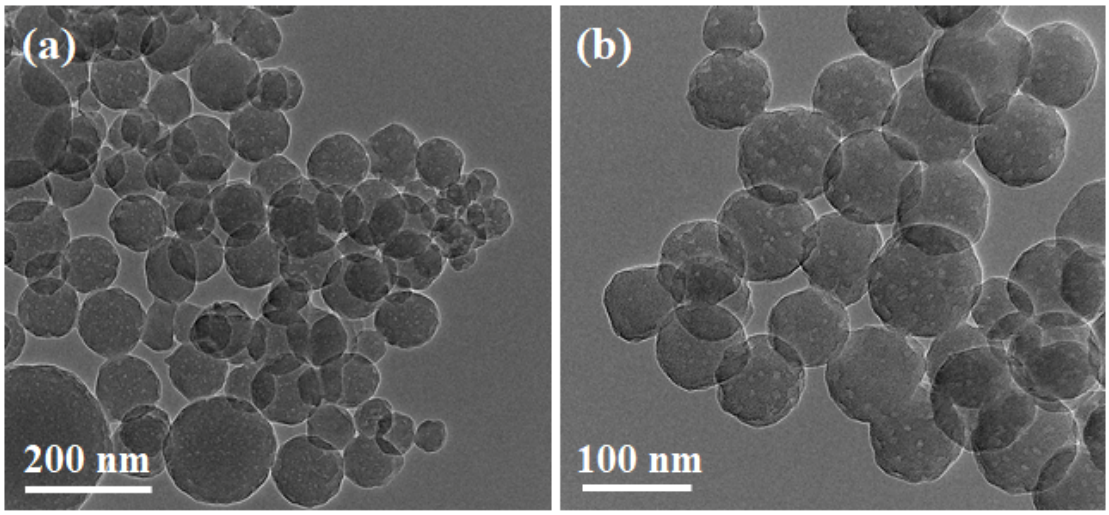

Fig. S8 TEM images of the sample were prepared by 2,4-DA participants in the reaction.

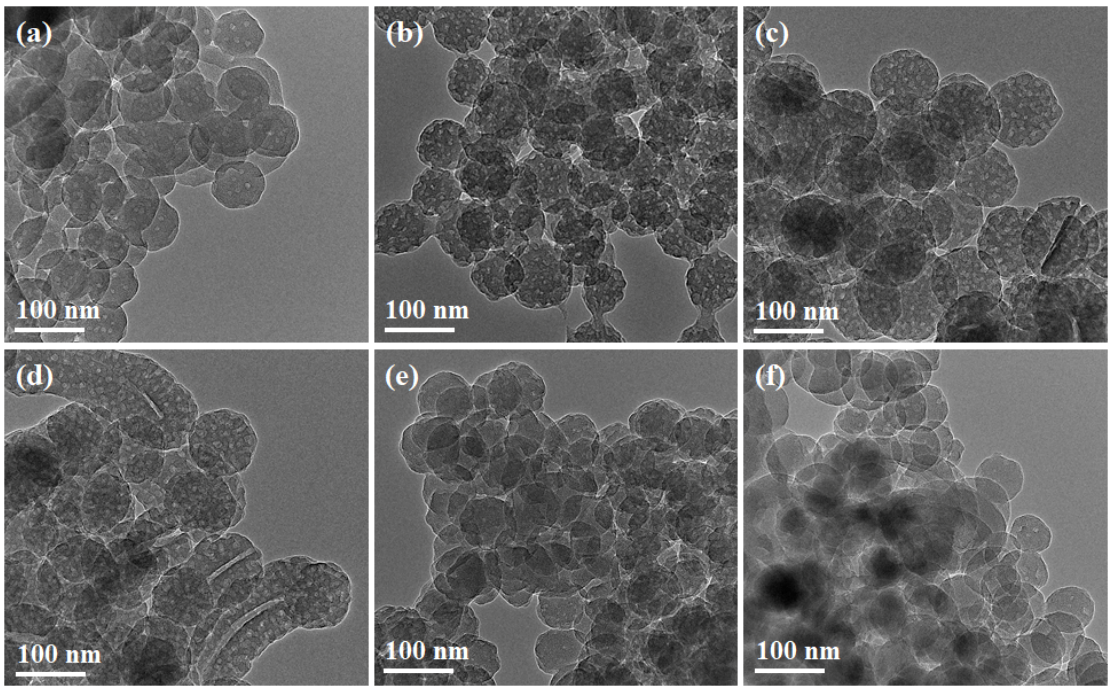

Fig. S9 TEM images of samples prepared by other types of composite surfactants: (a) SO-F127, (b) SL-P123, (c, d) SS-P123, (e) SLS-P123, and (f) SDBS-P123.

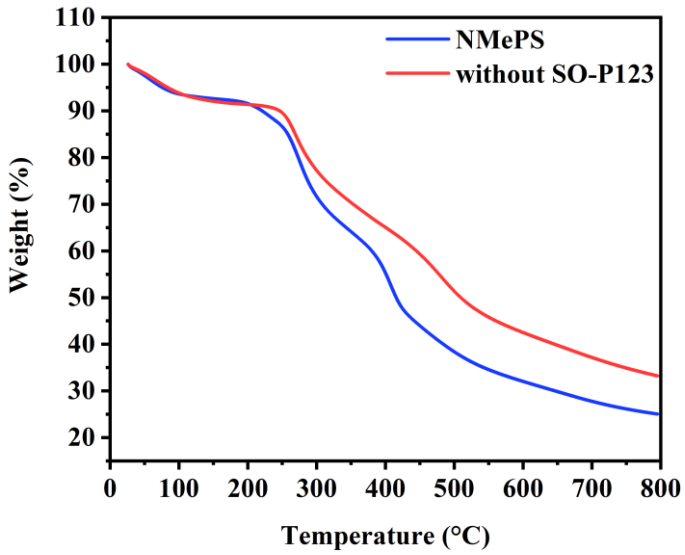

Fig. S10 TGA curves of NMePS and NPS.

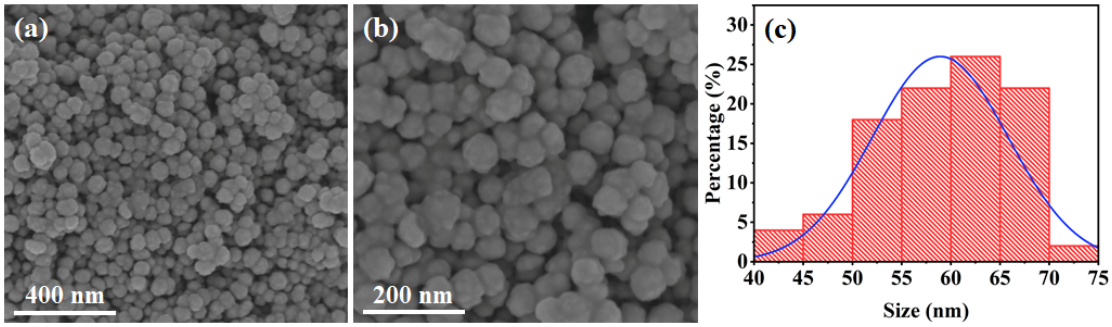

Fig. S11 (a, b) SEM images and (c) particle size distribution of NMeCS.

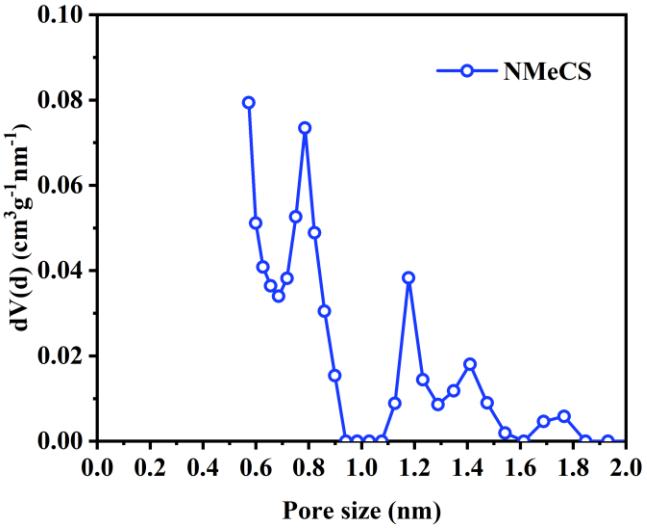

Fig. S12 Micropore size distribution curve of NMeCS calculated by the NLDFT model.

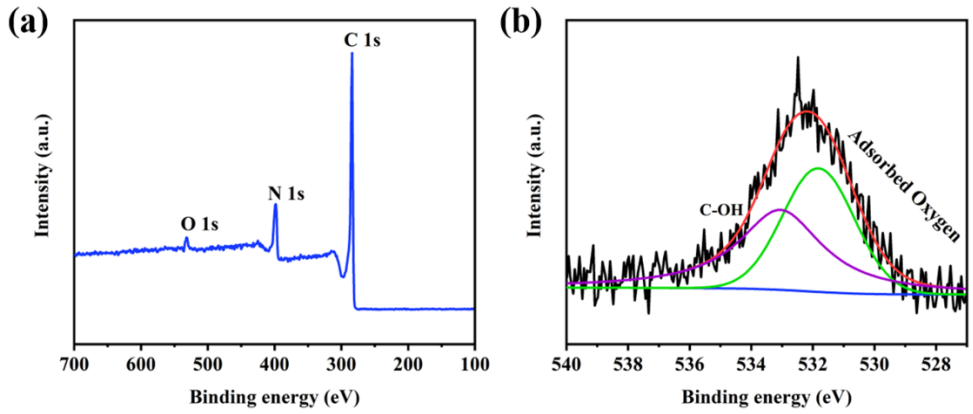

Fig. S13 (a) XPS survey and (b) O 1s spectrum of NMeCS.

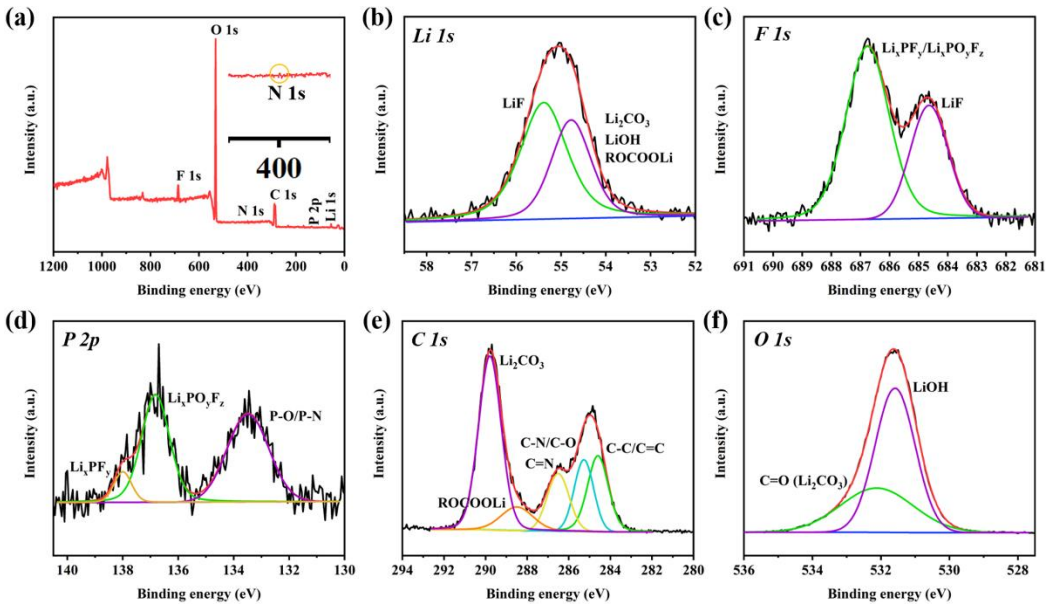

Fig. S14 (a) XPS survey, (b) Li 1s, (c) F 1s, (d) P 2p, (e) C 1s, and (f) O 1s deconvolution spectra of NMeCS electrodes after cycling.

To reveal the composition of the SEI layer, complete XPS survey of the NMeCS electrodes are performed and characteristic peaks belonging to Li 1s, F 1s, P 2p, C 1s, N 1s and O 1s can be observed (Fig. S14a). The Li 1s spectrum can be deconvoluted into two broad peaks corresponding to Li_2CO_3/LiOH/ROCOOLi and LiF species at 54.8 eV and 55.4 eV, respectively (Fig. S14b)[1]. The F1s spectrum discloses peaks that can be attributed to LiF (684.6 eV) and Li_xPF_y/$Li_xPO_yF_z$ (686.8 eV) species information, respectively (Fig. S14c)[2]. The peaks at 133.5 eV, 136.8 eV and 138.0 eV resolved from P 2p spectrum can be assigned to P-O/P-N, $Li_xPO_yF_z$ and Li_xPF_y, respectively (Fig S14d)[3]. Further, the peaks corresponding to newly generated species ROCOOLi (288.5 eV $^{C\ 1s}$), Li_2CO_3 (289.8 eV $^{C\ 1s}$, 532.1 eV $^{O\ 1s}$), and LiOH (531.6 eV $^{O\ 1s}$) can be dissected from the C 1s and O 1s spectra (Fig S14e, f)[1]. Based on the above discussion, it can be concluded that the main components of the SEI layer may include LiF, Li_2CO_3, LiOH,

ROCOOLi, Li_xPF_y and $Li_xPO_yF_z$.

In addition, the nitrogen content of the NMeCS electrode decreased from the original 14.97 at. % to 0.35 at. % before and after cycling, with an increase in Li (28.54 at. %), P (0.71 at. %) and F (3.81 at. %) content. As shown in S14a, the N 1s peak almost disappears, which is consistent with the literature reports[2].

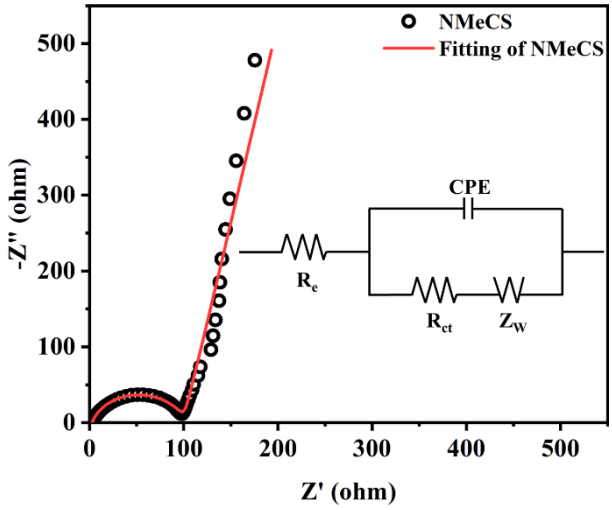

Fig. S15 Nyquist plot of NMeCS-based electrode, the solid red line indicates the fitting result (Inset is the equivalent circuit model).

The CPE (constant phase element) represents the capacitance of the SEI films and the double-layer capacitance, and Z_W is related to the Warburg resistance.[4]

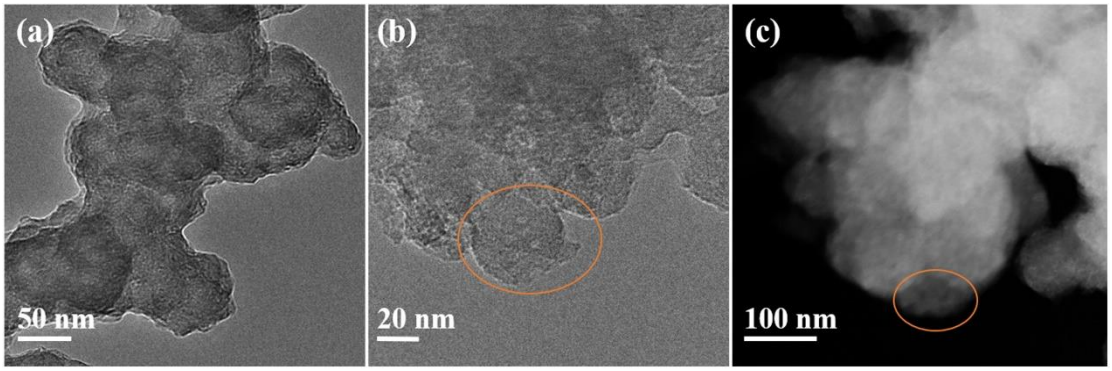

Fig. S16 (a, b) TEM and (c) STEM images of NMeCS electrodes after cycling.

As shown in Fig. S15, with the formation of SEI coating, there is adhesion between particles, but the spherical morphology of NMeCS can be maintained. Due to the blurring of the SEI layer, mesoporous structures can be observed in relatively thin regions of the tested samples.

Table S1 Electrochemical properties of several carbon materials for LIBs anode

Materials	Initial discharge/charge capacity (mA g^{-1})	Reversible capacity (mA h g^{-1})/number of cycles	Current density (mA g^{-1})	Ref.
NGS-5	638/413.7	400.6/100	100	5
SGNS-I	720/518.4	530.6/100	100	6
HGFs	443.7/375.1	338.9/50	50	7
CNCs	378.5/368.2	385.5/105	50	7
IMP-GC	706/455	400/100	100	8
PCS	734.9/721.2	386.5/100	50	9
CCL	500/-	400/100	50	10
A-900	579/403	318.8/100	100	11
NMeCS	732.3/470.7	383.7/100	100	This work

References

1 X. Chen, Y. Huang, K. Zhang, X. Feng and M. Wang, *Chem. Eng. J.*, 2017, **330**, 470-479.

2 J. S. Samdani, T.-N. Tran, T.-H. Kang, B.-J. Lee, Y. H. Jang, J.-S. Yu and S. Shanmugam, *J. Power Sources*, 2021, **483**, 229174.

3 H. Lee, H.-S. Lim, X. Ren, L. Yu, M. H. Engelhard, K. S. Han, J. Lee, H.-T. Kim, J. Xiao, J. Liu, W. Xu and J.-G. Zhang, *ACS Energy Lett.*, 2018, **3**, 2921-2930.

4 X. Qian, F. Zhang, Y. Zhao, K. Liang, W. Luo and J. Yang, *Front. Energy Res.*, 2020, **8**, 140.

5 P.-J. Yen, P. R. Ilango, Y.-C. Chiang, C.-W. Wu, Y.-C. Hsu, Y.-L. Chueh and K.-H. Wei, *Mater. Today Energy*, 2019, **12**, 336-347.

6 B. Guo, K. P. Ananth, J. Zhang, X. Ji and J. Bai, *Ionics*, 2020, **26**, 3267-3274.

7 L. Wang, Z. Liu, Q. Guo, G. Wang, J. Yang, P. Li, X. Wang and L. Liu, *Electrochim. Acta*, 2016, **199**, 204-209.

8 S. Sekar, Y. Lee, D. Y. Kim and S. Lee, *Nanomaterials*, 2019, **9**, 871.

9 Z. Chen, Y. J. Du, Z. H. Zhang, T. Gao and H. B. Li, *Nanotechnology*, 2019, **30**, 495403.

10 S. Li, Z. Jiang, A. Liu, J. Lu, J. Du, Y. Tao, Y. Cheng and H. Wang, *Int. J. Biol. Macromol.*, 2022, **222**, 1414-1422.

11 X. Liu, H. Tao, C. Tang and X. Yang, *Chem. Eng. Sci.*, 2022, **248**, 117200.